

# Estimation of the Ageing of Metallic Layers in Power Semiconductor Modules Using the Eddy Current Method and Artificial Neural Networks

Tien A. Nguyen<sup>1</sup>, Pierre-Yves Joubert<sup>2, \*</sup>, and Stéphane Lefebvre<sup>1</sup>

**Abstract**—In high power operations, the ageing of power semiconductor modules has been often observed by several failures due to high temperature cycling. The main failures may be metallization reconstruction, solder delaminations, bond wire lift-offs or bond wire heel crackings, conchoidal breaking of ceramics. The paper focuses on the non-contact monitoring of the ageing of the aluminum metallization top layer and of the solder bottom layer of a power die, using the eddy current method. The ageing is assumed to induce a decrease of these layers conductivity. The evaluation of both layers conductivity changes are estimated using artificial neural networks starting from eddy current data provided by finite element computations carried out in the case of several aged die configurations. The error of estimation is less than a few percent in the considered cases and it demonstrates the relevance of the eddy current method to monitor the ageing state of power modules. The proposed approach provides relevant results which will be validated on experimental data in future works.

## 1. INTRODUCTION

Electronic power modules are widely used for energy processing purposes, and their development extends to more and more industrial domains, such as automotive or aeronautics, with increasing demands in terms of reliability. Standard power modules are constituted of semiconductor dies soldered on direct copper bonded (DCB) ceramic substrate, as shown in Figure 1. Inside power modules, electrical connections are made by soldering or wire bonding between metallized layers. In addition, the DCB is implanted on a metallic base plate used as a mechanical support as well as a thermal cooler. The upper side of the modules is covered with an insulating silicone gel used to avoid partial discharges within the module. As a result, these modules are constituted of stacks of materials of various natures featured by various electro-mechanical properties. They include semiconductors, electrically conductive materials (metallic layers, solder layers. . .), and insulators (silicone gels, ceramics).

In many applications, power modules have to operate within variations of the ambient temperature, referred as passive temperature cycles [1, 2], which may reach high amplitudes. For instance, the environment temperature may rise to 120°C in the automotive application, or even to 200°C in the vicinity of aircraft jet engines. Furthermore, power modules are submitted to so-called active temperature cycles, which are relative to temperature variations resulting from their own power dissipation [1, 2]. Due to the different thermal expansion coefficients of the materials constituting the power modules, the thermal cycles induce mechanical stresses which may result in various types of degradations, such as solder delaminations, bond wire lift-offs and heel cracking, ceramics conchoidal fractures, or metallization reconstruction [1–6].

---

*Received 16 September 2014, Accepted 17 October 2014, Scheduled 19 December 2014*

\* Corresponding author: Pierre-Yves Joubert (pierre-yves.joubert@u-psud.fr).

<sup>1</sup> SATIE, ENS Cachan, CNAM, CNRS, 61 Avenue du Pdt Wilson, Cachan 94235, France. <sup>2</sup> IEF, Université de Paris-Sud, CNRS, Centre Scientifique d'Orsay, Orsay F-91405, France.

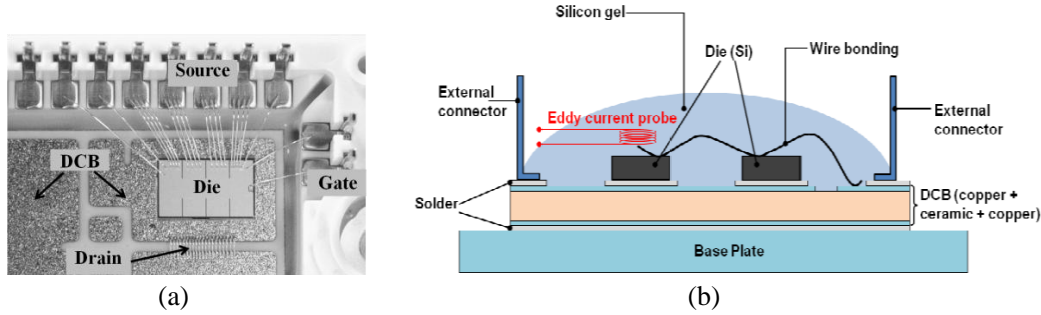


**Figure 1.** Multilayered conductive structure of power semiconductor module, (a) top view of a typical module, (b) schematic cut view.

Therefore, the analysis and evaluation of the degradation process is a key issue for optimizing the use of power modules as well as for preventing failures. In particular, the degradation of the metallized layers of chips has been highlighted by many authors as a major source of failure [1, 2, 6]. As a result, the non-destructive evaluation (NDE) of such layers may help to better understand the alteration process, and subsequently, to foresee and prevent failures.

The eddy current (EC) method allows the quantitative NDE of metallic layers to be carried out [7], and hence, it is a good candidate to evaluate the ageing state of chip metallization and solder layers. Furthermore, the method is easy to implement, non contact, robust, and suitable to *in situ* NDE applications, providing EC micro-sensors [8] are considered. Previous works carried out by the authors have shown that EC methods can quantitatively diagnose the state of thermally-aged  $4\ \mu\text{m}$  aluminum single layers deposited on a silicon bulk [9]. The same authors have also experimentally highlighted that the EC technique implemented in a wide frequency range was relevant to qualitatively sense the ageing state of different conducting layers in an actual power module sample [10].

In this study, the authors aim at assessing the feasibility of the quantitative EC NDE of the ageing state of multiple conductive layers of an aged power module die. To do so, a typical transistor chip soldered on a DCB substrate is considered. For this chip, the alteration of the upper aluminum metallization and the bottom-side soldering layer are jointly considered. Since it is difficult to obtain module samples featuring such layers of adjustable ageing state, data only provided by finite element (FE) computations are considered in this study. In order to evaluate the feasibility of the method, computed data relative to the interactions between a mini-cup-core bobbin-coil EC sensor and a transistor featured by adjustable ageing parameters are used. Parametric computations enable data relative to various ageing states to be provided. These data are firstly used to analyze and evaluate the sensitivity of the EC method to multiple layer alterations. They are used secondly to feed an artificial neural network (ANN) [11] so as to elaborate an able estimator to evaluate the ageing parameters of the considered transistor layers, starting from the available EC data. In the second section of this paper, the considered transistor sample and the implemented EC method are presented. Then, the implementation of the FE computations is described and obtained results are discussed. In Section 3, the elaboration of the used ANN and the estimation of transistor ageing state using the ANN are addressed. Conclusions are presented in Section 4.

## 2. IMPLEMENTATION OF THE EC NDE OF AN AGED TRANSISTOR CHIP

### 2.1. Basic Principles of the EC Method Used

The eddy current (EC) method has been used for the NDE of electrically conductive parts for many decades [7]. Indeed, EC NDE is a rather popular method since it is easy to implement, contactless and sensitive to the geometric and electric parameters of the part under test. The most basic EC sensor configuration is given by a single bobbin coil (possibly associated with a ferrite core) fed by a time harmonic current and used as a transmit and receive probe. When such a coil probe is placed near to the part to be tested, the magnetic field generated by the probe induces eddy currents within the part. The resulting electromagnetic coupling between the probe and the part depends on the measurement

distance (lift-off) and on the properties of the part. These parameters may be sensed through the impedance changes measured at the ends of coil. The EC data used in this study are the complex normalized impedance  $Z_n$  of the probe, which can be expressed as [12]:

$$Z_n = R_n + jX_n = \frac{R - R_0}{X_0} + j\frac{X}{X_0} \quad (1)$$

where  $R_0$  and  $X_0$  are the resistance and the reactance of the uncoupled probe respectively, and  $R$  and  $X$  are respectively the resistance and the reactance of the complex impedance of the probe when coupled to the test part. The use of  $Z_n$  is more relevant than the use of the impedance  $Z = R + jX$  of the coupled probe because it enables getting rid of the influence of the constitution of the probe (losses  $R_0$  and self reactance  $X_0$  of the coil winding [12]) to focus on the impedance changes due to the tested part. Indeed, the normalized impedance  $Z_n$  only depends on the used excitation frequency, the electromagnetic properties (electrical conductivity  $\sigma$ , magnetic permeability) and the geometric properties of the part (sensor lift-off, layer thickness) [13].

In the case of large massive metallic parts of known thickness, it has been established that the normalized impedance of the sensor coupled to the part may be expressed using a simple analytical coupling model based on the analogy to an electrical transformer [12, 13]. This model enables to foresee the frequency responses of  $Z_n$  according to the geometric and electromagnetic properties of the investigated material. It also allows the universal impedance diagram (UID), which is the evolution of  $Z_n$  plotted in the  $(R_n, X_n)$  complex plane, to be plotted for frequencies ranging from 0 to infinity [12]. For massive plane parts, the UIDs feature expected patterns. In practice, these expected patterns can be used to estimate the part parameters starting from EC data provided in adequate frequency bands. In the case of a thin aluminum film deposited on a silicon substrate, the authors have shown in [9] that the ageing state of the thin film may be quantified starting from the alterations of the UID resulting from the modifications of its conductivity with thermal fatigue. Moreover, the authors have experimentally pointed out that the frequency response  $Z_n$  of a commercial EC sensor being implemented in the 5 Hz–2.5 MHz bandwidth was relevant to sense the ageing of metallic layers in power semiconductor module [10]. Indeed, at low frequencies, the obtained EC data were found to be sensitive to the ageing state of the solder layer and the DCB substrate of the power module. Conversely, at high frequencies, due to skin effect in the metallic layers [7], the EC data were found to be mainly related to the power module chip, and more specifically to the metallized top layer of the chip [10]. However, these preliminary experimental results only enable to assess the effects of the metallization ageing. The actual ageing state evaluation requires one i) to develop an accurate modeling tool of the interactions between the EC probe/power module [14, 15] and ii) to solve the inverse problem so as to estimate the value of the metallization conductivity starting from the collected EC data.

In order to assess the feasibility of the quantitative EC estimation of the ageing state of multiple conducting layers of the die, in this study the authors have chosen to turn to FE modeling to provide EC data related to multilayer aged specimens. The implementation of such FE computations is presented in the following subsection.

## 2.2. Simulation of Electromagnetic Coupling between EC Probe and Power Semiconductor

In this section, finite element (FE) computations of the EC testing of a typical power module transistor chip are reported. To do so, a cup-core bobbin coil sensor (NORTEC<sup>†</sup> 3551F-1 MHz) commercialized by NORTEC is considered. The coils have an effective sensitive area of approximately 2 mm in diameter. The preferred frequency range is from 1 MHz to 2 MHz.

Assuming that the used EC sensor is of sufficiently small radius comparatively to the transistor chip surface ( $6.59 \times 10.52 \text{ mm}^2$ ), the whole simulation workspace may be considered as being axisymmetric. Therefore two-dimensional (2D) electromagnetic computations are carried out using 2D ANSYS<sup>‡</sup> software. A standard power semiconductor module consists of a silicon die, a DCB substrate, and a base plate. The silicon die is made of a thin aluminum metallization layer, a low doping silicon layer

<sup>†</sup> <http://www.olympus-ims.com/en/ec-probes/>

<sup>‡</sup> <http://www.ansys.com/>

(epitaxial layer), and a high doping silicon layer (substrate). The die is soldered to the DCB substrate. The resultant solder layer is around  $80\ \mu\text{m}$ . The dimensions and constitutive parameters of each layer have been chosen as close as possible to the ones of a typical power module (e.g., MOSFET module fabricated by Microsemi [10]). Dimensions and features are gathered in Table 1 and the corresponding computational axisymmetric workspace is depicted in Figure 2.

In order to implement the FE computations, a quasi static analysis is used featuring FE element PLANE13 in the ANSYS software. The harmonic model uses the magnetic vector potential formulation to solve the eddy current region and each node of the elements owns a magnetic vector potential as degree of freedom. Here we chose a quadrilateral element featuring 4 nodes in rotational axisymmetry (Figure 2).

Magnetic boundary conditions are applied to the exterior boundaries of the workspace. The  $Y$  axis

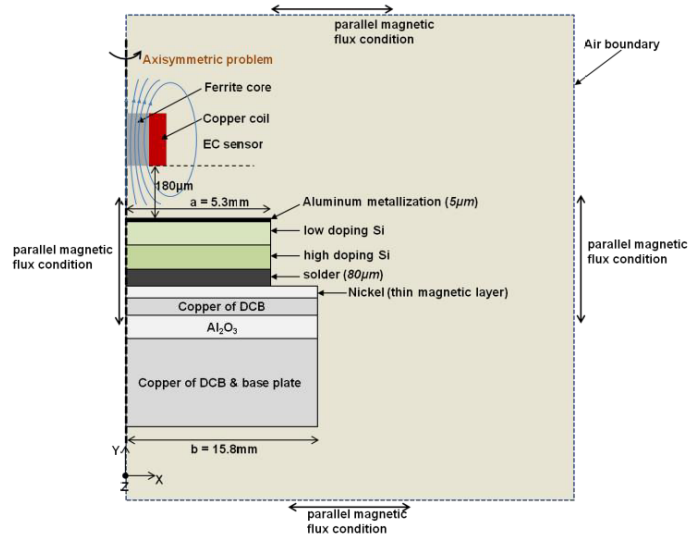


**Figure 2.** Simulation of multilayered structure of power semiconductor module.

**Table 1.** Dimensions and physical parameters of layers in the simulated structure.

Layer \ Parameter	Thickness ( $\mu\text{m}$ )	Width (mm)	Electrical conductivity ( $\text{S}\cdot\text{m}^{-1}$ )	Relative magnetic permeability
Aluminum metallization	5	5.3	$37.7 \times 10^6$	1
Low doping Silicon	50	5.3	25	1
High doping silicon	170	5.3	$0.25 \times 10^6$	1
Solder	80	5.3	$6.67 \times 10^6$	1
Nickel	4	15.8	$14.4 \times 10^6$	200
Upper copper of DCB	300	15.8	$60 \times 10^6$	1
Ceramic	380	15.8	$1 \times 10^{-17}$	1
Lower copper of DCB and base plate	3000	15.8	$60 \times 10^6$	1

represents the rotational symmetry axis. The parallel flux condition is applied to this axis. Also, the open boundaries are set to parallel flux conditions. Figure 2 shows the magnetic flux parallel condition at the  $y$ -axis of the model and at the open boundaries.

The procedure of data extraction will be described below. The FE computation allows simulating the magnetic flux ( $\psi$ ) going through the sensor core. The electromotive force ( $EMF$ ) induced at the ends of the sensor coil is calculated as follows:

$$EMF = j \cdot 2 \cdot \pi \cdot f \cdot \psi \tag{2}$$

where  $f$  is the excitation frequency,  $j$  is the imaginary unit.

Then the impedance  $Z$  of the sensor ( $Z = R + j \cdot X$ ) is determined with the expression given by:

$$Z = \frac{EMF}{I} \tag{3}$$

where  $I$  is the excitation current.

The normalized impedance ( $Z_n$ ) is then computed using Eq. (1) after FE computations of the sensor in unloaded and loaded configurations.

In the considered FE workspace, the material parameters which are modified by the ageing process are the electrical conductivity of both the power die aluminum layer and the solder layer between the power die and the DCB substrate. For the initial state of the power module, the aluminum conductivity  $\sigma_{al}^0$  has been set to the value of bulk aluminum, i.e.,  $\sigma_{al}^0 = 37.7 \text{ MS}\cdot\text{m}^{-1}$ . In the same way, the solder conductivity  $\sigma_{solder}^0$  at initial state is set to be equal to the conductivity of Sn<sub>63</sub>Pb<sub>37</sub> alloy, widely used in the standard power modules, i.e.,  $\sigma_{solder}^0 = 6.67 \text{ MS}\cdot\text{m}^{-1}$ . Then, the ageing of both layers are simulated by decreasing the conductivity of these layers. The reduction factors are denoted  $\alpha_{al}$  and  $\alpha_{solder}$  for the aluminum and solder layers, respectively. They are such that:

$$\begin{aligned} \sigma_{al} &= \frac{\sigma_{al}^0}{\alpha_{al}} \\ \sigma_{solder} &= \frac{\sigma_{solder}^0}{\alpha_{solder}} \end{aligned} \tag{4}$$

In this study,  $\alpha_{al}$  ranges from 1 to 19, and  $\alpha_{solder}$  ranges from 1 to 11, these values being estimated to be realistic, considering previous experimental evaluations [9, 10]. These variations lead to a large set of possible ageing configurations. Figure 3 provides some examples of UID computed in the 5 Hz–2.5 MHz bandwidth for sound and aged configurations.

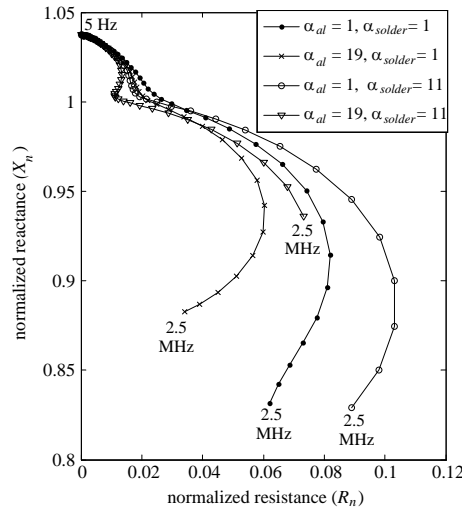


**Figure 3.** Universal Impedance Diagram (UID) of EC normalized impedance for the three ageing states and an initial state of aluminum and solder layer for a power semiconductor module.

In Figure 3 the initial state ( $\alpha_{al} = 1, \alpha_{solder} = 1$ ), two intermediate ageing states ( $\alpha_{al} = 1, \alpha_{solder} = 11$ ), ( $\alpha_{al} = 19, \alpha_{solder} = 1$ ), and the most advanced ageing state ( $\alpha_{al} = 19, \alpha_{solder} = 11$ ) are considered. The UID obtained of the most considerable ageing state has the smallest local radius at low frequencies and the shortest length, the UID featuring the smallest radius at high frequencies corresponds to the ageing state of only conductivity variation of aluminum layer ( $\alpha_{al} = 19, \alpha_{solder} = 1$ ), and the UID corresponding the only conductivity variation of solder layer ( $\alpha_{al} = 1, \alpha_{solder} = 11$ ) has the greatest radius at high frequencies. It isn't easy to claim the behavior change of UID in the case of the ageing state of both these layers jointed. However, theoretically, we can note that the low frequency part of UID is mainly related to the solder and substrate layers, and that the high frequency part of UID is mainly related to the die. Indeed, at high frequencies, the EC induced in the substrate are strongly reduced by the aluminum and solder layers which are highly conductive. This is why the substrate is hardly sensed by the E probe at these frequencies. From these examples, one may conclude that a relevant frequency band may be determined to select EC data for ageing evaluation purposes.

### 2.3. EC Data for the Estimation of Ageing

In order to estimate the conductivity variations of the power die aluminum and solder layers, the variations of the normalized impedance between the ageing state and the initial state, denoted  $\Delta Z_n$  is defined as:

$$\Delta Z_n = Z_n(\alpha_{al}, \alpha_{solder}) - Z_n(\alpha_{al}^0, \alpha_{solder}^0) \quad (5)$$

where  $Z_n(\alpha_{al}^0, \alpha_{solder}^0) = Z_n(1, 1)$  is the normalized impedance obtained at initial state.

The variations of the real and imaginary parts of  $\Delta Z_n(f)$  versus frequency are presented in Figures 4

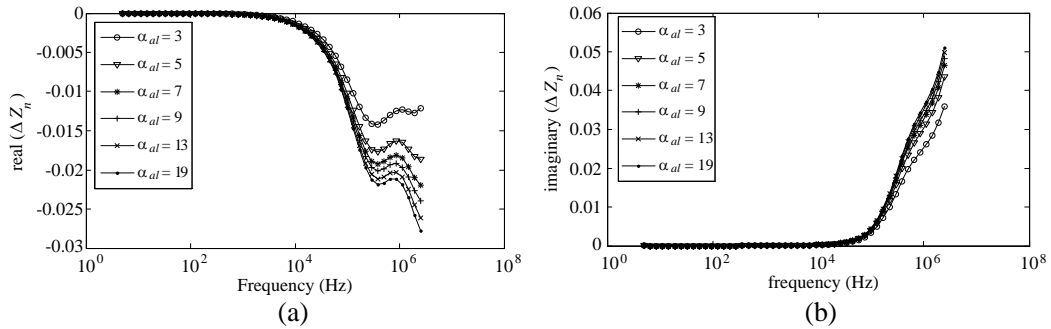


**Figure 4.**  $\Delta Z_n$  as a function of the excitation frequency for several values of the conductivity of the aluminum layer, the solder conductivity being fixed at the initial state, (a) real part of  $\Delta Z_n$ , (b) imaginary part of  $\Delta Z_n$ .

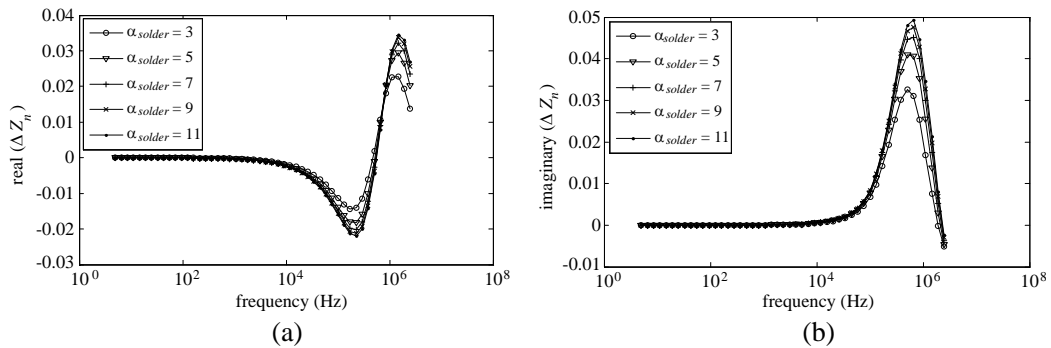


**Figure 5.**  $\Delta Z_n$  as a function of the excitation frequency for several values of the solder conductivity, the aluminum layer conductivity being fixed at the initial state, (a) real part of  $\Delta Z_n$ , (b) imaginary part of  $\Delta Z_n$ .

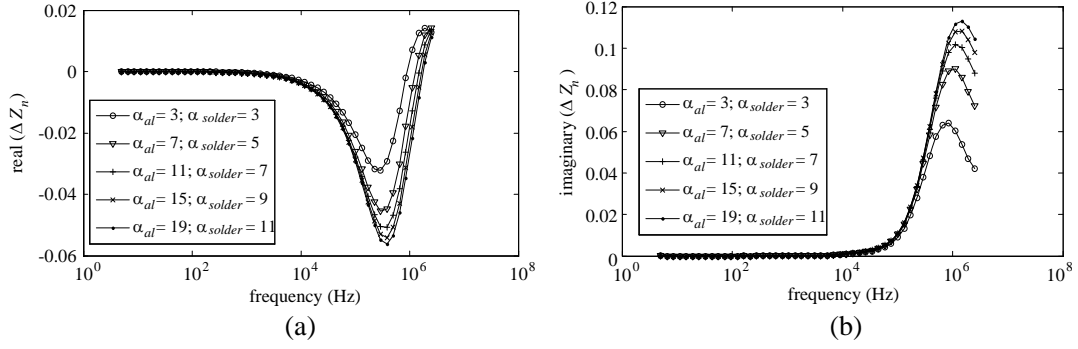


**Figure 6.**  $\Delta Z_n$  as a function of the excitation frequency for several values of the aluminum layer conductivity and of the solder layer conductivity, (a) real part of  $\Delta Z_n$ , (b) imaginary part of  $\Delta Z_n$ .

to 6 for various ageing configurations. Figure 4 illustrates the influence of the aluminum conductivity ( $\sigma_{al}$ ) on the variations of  $\Delta Z_n(f)$ , the aluminum layer is successively altered by six attenuation values  $\alpha_{al} = [3, 5, 7, 9, 13, 19]$ , while the solder conductivity is fixed at initial state ( $\alpha_{al} = 1$ ). In the same manner, Figure 5 illustrates the influence of the solder layer conductivity,  $\sigma_{solder}$  (with  $\alpha_{solder} = [3, 5, 7, 9, 11]$ ) on the variations of  $\Delta Z_n(f)$ , the aluminum conductivity is fixed at initial state ( $\alpha_{al} = 1$ ). Finally, Figure 6 shows the influence of both conductivity variations on  $\Delta Z_n(f)$  for  $(\alpha_{al}, \alpha_{solder})$  taking values such as (3, 3); (7, 5); (11, 7); (15, 9); and (19, 11). These graphs point out that there exists a relevant frequency band which enhances the sensitivity of the EC sensor to the conductivity changes. In what follows, the frequency band ( $FB$ ) used for estimation purposes is set to  $FB = [11.8 \text{ kHz} - 2.5 \text{ MHz}]$ .

In addition, noisy EC data are considered in this study. Indeed, based on previous experiments [10], EC data measured with the NORTEC sensor on such a power module structure feature a signal to noise ratio (SNR) close to 60 dB. So as to be more realistic in this study, computed EC data have been altered by additive white noise standing for so electronic noise as well as measurement uncertainties such as sensor positioning repeatability [16]. This additive noise is added in equal proportion to both the real and the imaginary parts of  $\Delta Z_n$  so that [17]:

$$SNR = 20 \times \log_{10} \left( \frac{\max |\Delta Z_n|}{\sqrt{\lambda_{real}^2 + \lambda_{imag}^2}} \right) \quad (6)$$

where  $\lambda_{real}$  and  $\lambda_{imag}$  are the standard deviations of the noise altering the real and imaginary parts of  $\Delta Z_n$ , respectively. Starting from these noisy EC data, the evaluation of the conductivity variations of aluminum and solder layer using artificial neural network is implemented in the following section.

### 3. EVALUATION OF CONDUCTIVITY VARIATION OF ALUMINUM AND SOLDER LAYER USING ARTIFICIAL NEURAL NETWORK

The goal of this study is to estimate the variations of the aluminum conductivity ( $\sigma_{al}$ ) and solder conductivity ( $\sigma_{solder}$ ) during the ageing process. In order to bypass the difficulties of inverting a numerical model to estimate these parameters starting from EC data [18], a model-free estimation technique based on the use of an ANN is considered. This kind of approach has been proven to be efficient in various modeling and estimation problems in the electromagnetic domain [19, 20]. In this study, a feed-forward neural network (FFNN) is implemented to estimate the conductivity variations [21]. This particular ANN was found relevant in several eddy current estimation problems [22, 23]. In this paper, the authors use the neural network toolbox of Matlab to implement the FFNN estimation [24].

To do so, the available noisy EC data are divided into three data sets: the training database, the validation database and the test database. These different datasets are used to separately optimize the weights, the biases and the size of the ANN (number of neurons of the hidden layer). The training database is used to feed the network during training process, and the network parameters are adjusted

according to the estimation errors observed in known configurations. The validation database is used to measure network generalization ability and to halt training process when generalization stops improving. The testing database has no effect on the training. It is used to provide an estimation of the network performances during and after training [24].

### 3.1. Elaboration of the FFNN for Estimating Conductivity Variations

The inputs of FFNN consist of the multi-frequency EC data  $\Delta Z_n$  obtained in various configurations of aged module. For each selected configuration, 21 different values of  $\Delta Z_n$  obtained for 21 frequencies logarithmically distributed in the frequency band  $FB$ , are considered.

Since the real and the imaginary parts of  $\Delta Z_n$  are separately considered, the FFNN is fed with a total amount of 42 inputs. The FFNN features two outputs, the estimated conductivity of the aluminum layer ( $\hat{\sigma}_{al}$ ) and the estimated conductivity of the solder layer ( $\hat{\sigma}_{solder}$ ). The used FFNN is finally set with a single hidden layer, as depicted in Figure 7.

Among the EC data provided by FE computations, the training and validation database has been created from the normalized impedance variations ( $\Delta Z_n$ ) of sixty configurations of ageing states. These sixty configurations correspond to the ten values of aluminum conductivity in the range of  $\alpha_{al} = [1, 3, 5, \dots, 19]$  given by the odd factors of  $\alpha_{al}$ , and the six values of solder conductivity in the range of  $\alpha_{solder} = [1, 3, 5, \dots, 11]$  given by the odd factors of  $\alpha_{solder}$ . Figure 8 illustrates these sixty configurations of ageing state selected in the first data set (training and validation process). Then we will chose the second data set (testing database) of ageing states which are different from the ageing states of the training and validation databases. The testing database has been made from  $\Delta Z_n$  values for nine configurations of ageing state which correspond to three values of aluminum conductivity in the range of  $\alpha_{al} = [8, 10, 12]$  given by the even factors of  $\alpha_{al}$  and three values of solder conductivity in the range of  $\alpha_{solder} = [4, 6, 8]$  given by the even factors of  $\alpha_{solder}$ . The testing databases allow us to calculate the estimation error of each built ANN.

After adding the noise to the EC data, each value of  $\Delta Z_n$  will be multiplied by  $M$  different values ( $M = 30$ ) around  $\Delta Z_n$  which ensures the signal-noise-ratio ( $SNR$ ) of 60 dB as defined in the Section 2.3. For the training and validation databases, the total number of input-output couples of EC data is equal to  $60 \times 30 = 1800$ . For the testing database, the total number of input-output couples is equal to  $9 \times 30 = 270$ . Each input-output couple of EC data is featured by 42 inputs consisting of the real and imaginary part of  $\Delta Z_n$  and 2 outputs relative to the actual values of conductivities  $\sigma_{al}$  and  $\sigma_{solder}$ .

Because the neural network minimization problem is often ill-conditioned, the ANN training process uses the back propagation Levenberg-Marquardt algorithm [25, 26], and its generalization ability was assessed according to a cross-validation procedure [27].

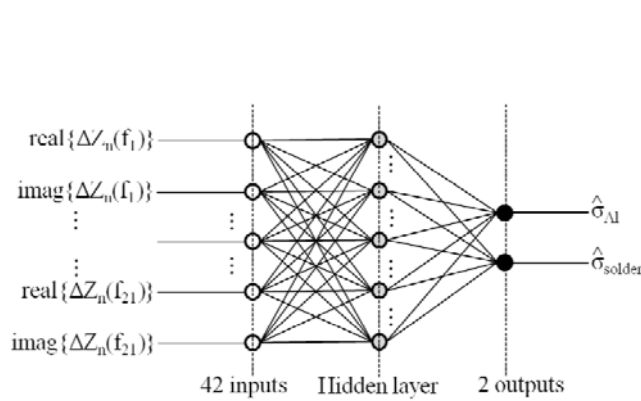


**Figure 7.** Fully connected feed-forward ANN with one hidden layer and one output layer used for the estimating the conductivity variation.

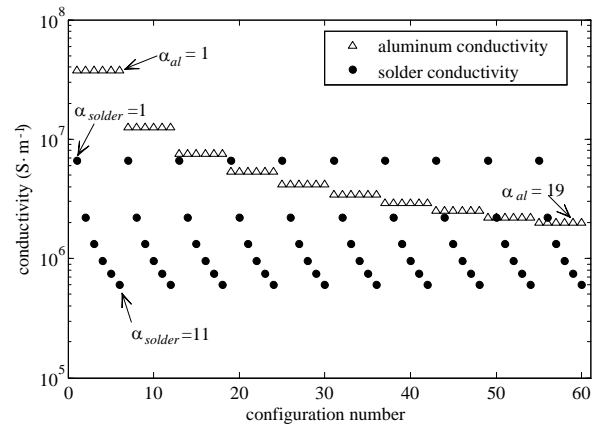


**Figure 8.** Sixty configurations of ageing states chosen for the training and validation database of ANN.

To do so, among 1800 input-output couples of the training and validation database, 1/6 of the data corresponding to the ageing states located in the limits of ageing ( $\alpha_{al} = 1$  and  $\alpha_{al} = 19$ ) have been dedicated to the validation process of ANN, the remaining data being dedicated to the training process of the ANN. In order to search for an optimized ANN we consider ANNs having the number of neurons in the hidden layer varying from 1 to 80. Then we select the network corresponding to the lowest estimation error. Using the testing database, the root mean square error (*RMSE*) between the estimated conductivities ( $\hat{\sigma}_{al}$  and  $\hat{\sigma}_{solder}$ ) and the actual conductivities ( $\sigma_{al}$  and  $\sigma_{solder}$ ) have been calculated for every network using:

$$RMSE = \sqrt{\frac{1}{N} \times \sum_{i=1}^N \left( \frac{1}{M} \times \sum_{j=1}^M (\hat{\sigma}_{ij} - \sigma)^2 \right)} \quad (7)$$

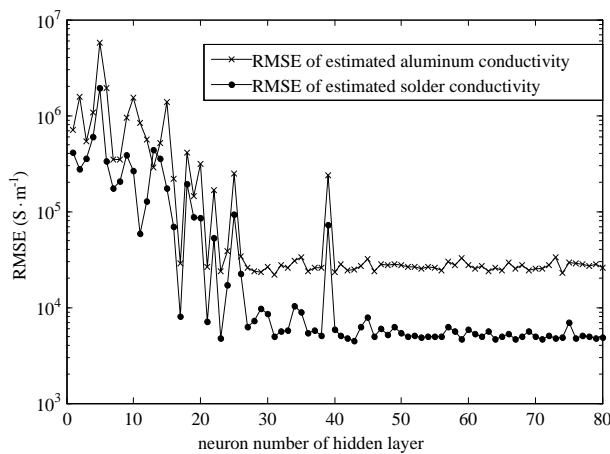
where  $M$  is the number of generated values simulating the added noise,  $M = 30$ ,  $N$  is the number of configurations of ageing state,  $N = 9$  with the testing database of the second data set.

Figure 9 shows the evolution of *RMSE* of  $\hat{\sigma}_{al}$  and  $\hat{\sigma}_{solder}$  calculated from the testing database as a function of number of neuron in the hidden layer. We can note that a hidden layer featuring 56 neurons is a good choice to keep the evaluation error as low as possible for the estimation of  $\sigma_{al}$  and  $\sigma_{solder}$ .

### 3.2. Estimation Results

Joint estimation of aluminum conductivity and solder conductivity has been performed by mean of the ANN selected in Section 3.1. In order to test the generalization capability of the chosen network, the testing database has been enlarged by the different ageing states that are located outside of the training and validation database. Now the new testing database corresponds to six values of aluminum conductivity in the range of  $\alpha_{al} = [8, 10, 12, 14, 16, 18]$  and three values of solder conductivity in the range of  $\alpha_{solder} = [4, 6, 8]$ . As a result, the new testing database is constituted of 18 ageing state configurations. The chosen frequency band and the noise power added to the EC data were the same as previously described. In order to quantify the estimation results, we define the estimate bias ( $\mu$ ) as the mean value of the estimated conductivity. The mean and the standard deviation of the values of the estimated conductivity (*std*) for  $M$  estimated values of each ageing configuration are given by:

$$\mu = \frac{1}{M} \times \sum_{k=1}^M \hat{\sigma}_k \quad (8)$$



**Figure 9.** Generalization of ANN for selecting the optimal network of estimation.

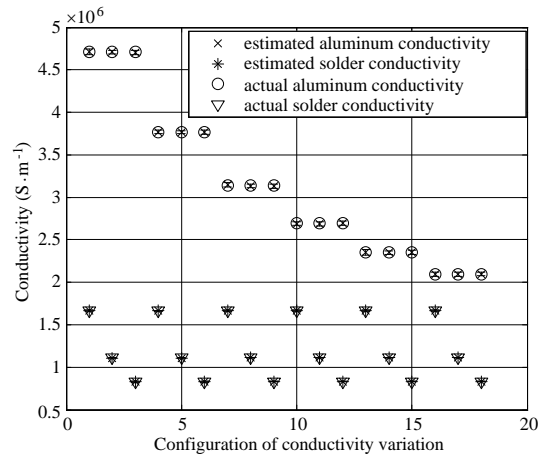


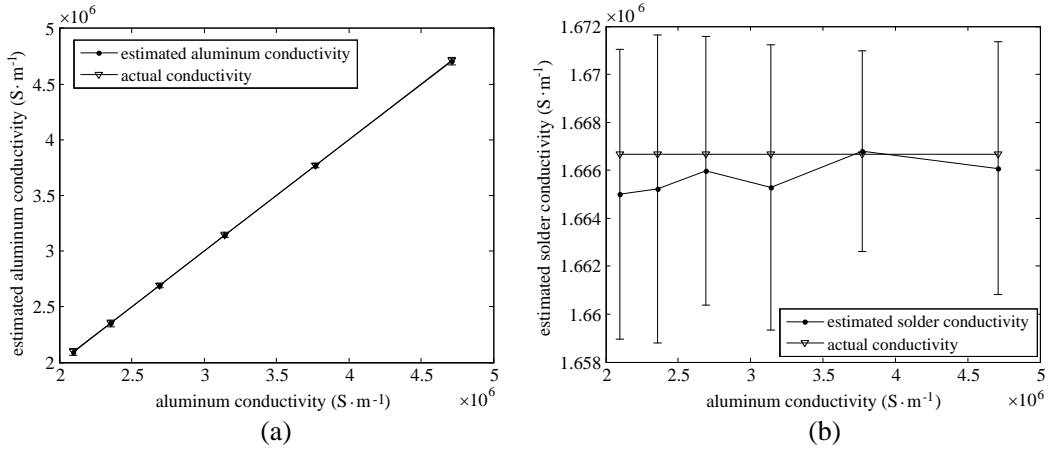
**Figure 10.** Comparison between estimated results and actual conductivity for all data sets of the test process.

$$std = \sqrt{\frac{1}{M-1} \times \sum_{k=1}^M (\hat{\sigma}_k - \mu)^2} \quad (9)$$

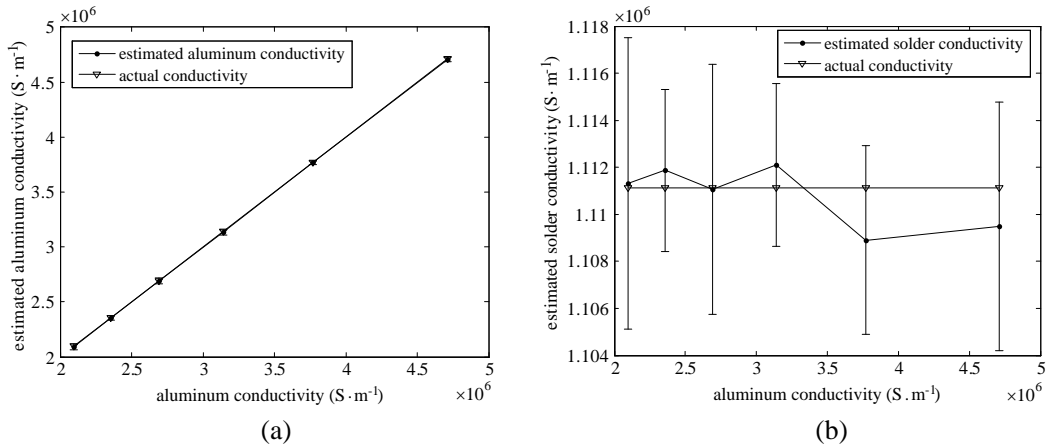
where  $\sigma$  and  $\hat{\sigma}$  represent the considered conductivity  $\sigma_{al}$  and  $\sigma_{solder}$  (true values) and its estimation respectively.  $M$  is still defined as the number of generated values simulating the added noise,  $M = 30$ .

Figure 10 illustrates all ageing configurations of the new testing database corresponding to the actual conductivities ( $\sigma_{al}$  and  $\sigma_{solder}$ ) and the estimated ones ( $\hat{\sigma}_{al}$  and  $\hat{\sigma}_{solder}$ ). The estimated conductivities are represented by their mean values  $\mu$  (Eq. (8)) with the error bar being equal to the standard deviation,  $std$  (Eq. (9)). One can note that the estimations are satisfactory with the very small deviations between the estimated and actual values of the conductivities.

Figures 11 to 13 represent the conductivity estimation when the solder conductivity has been fixed at the value corresponding to the factors of  $\alpha_{solder} = 4, 6, 8$  respectively and the aluminum conductivity is the value of new testing data corresponding to the factor of  $\alpha_{al} = [8, 10, 12, 14, 16, 18]$ . The solid lines represented on these figures link the points corresponding to the estimate bias (Eq. (8)) and the error bars plotted around these points show the estimation standard deviation (Eq. (9)). The dashed



**Figure 11.** Results of joint estimation of  $\sigma_{al}$  and  $\sigma_{solder}$  for  $\alpha_{al} = [8, 10, 12, 14, 16, 18]$  and  $\alpha_{solder} = 4$ , (a) estimation of aluminum conductivity, (b) estimation of solder conductivity. (The error bar corresponds to the standard deviation, centered on the estimate bias  $\mu$ ).



**Figure 12.** Results of joint estimation of  $\sigma_{al}$  and  $\sigma_{solder}$  for  $\alpha_{al} = [8, 10, 12, 14, 16, 18]$  and  $\alpha_{solder} = 6$ , (a) estimation of aluminum conductivity, (b) estimation of solder conductivity. (The error bar corresponds to the standard deviation, centered on the estimate bias  $\mu$ ).

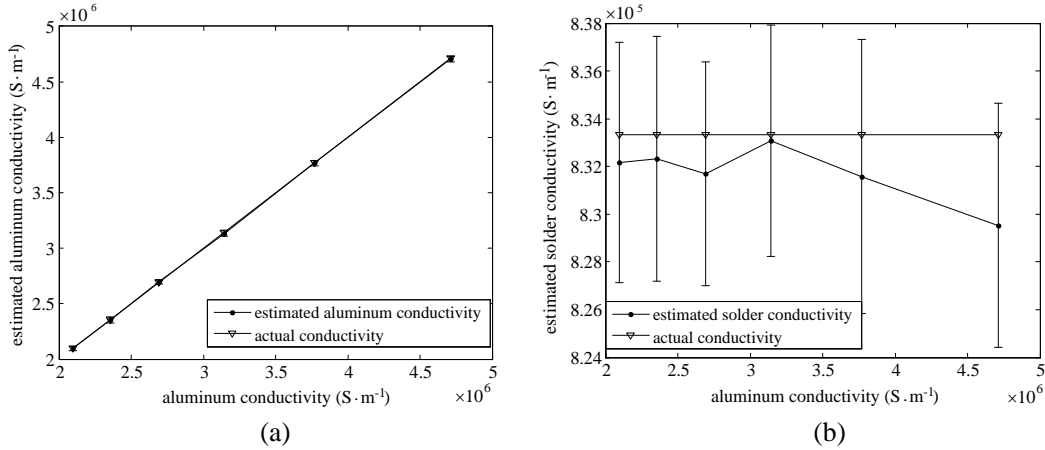


**Figure 13.** Results of joint estimation of  $\sigma_{al}$  and  $\sigma_{solder}$  for  $\alpha_{al} = [8, 10, 12, 14, 16, 18]$  and  $\alpha_{solder} = 8$ , (a) estimation of aluminum conductivity, (b) estimation of solder conductivity. (The error bar corresponds to the standard deviation, centered on the estimate bias  $\mu$ ).

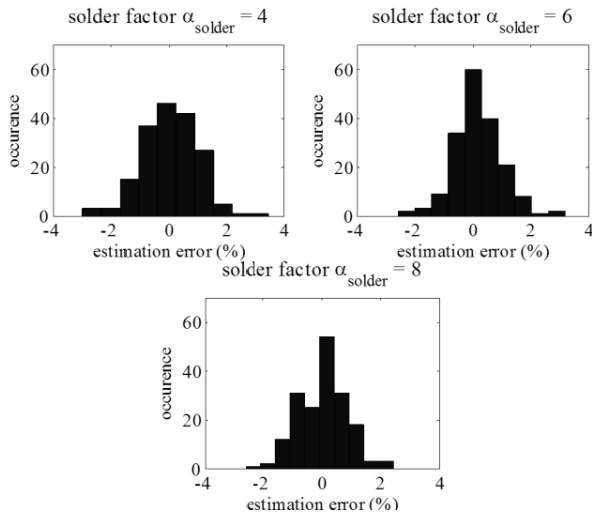


**Figure 14.** Histogram of estimation error for the aluminum conductivity.

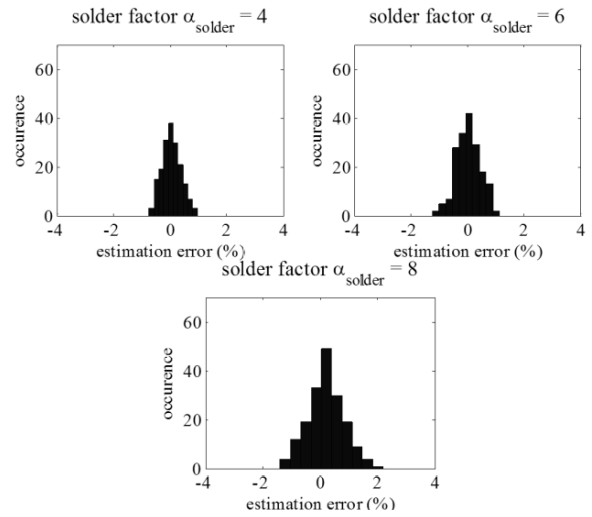


**Figure 15.** Histogram of estimation error for the solder conductivity.

lines link the points corresponding to the actual conductivities.

In addition, Figure 14 and Figure 15 illustrate the histogram of estimation errors. The error of estimation is calculated for all 540 input-output couples of the new testing data, the error of estimation being given by the following expression:

$$error = 100\% \times \frac{\hat{\sigma} - \sigma}{\sigma} \tag{10}$$

where  $\hat{\sigma}$  and  $\sigma$  are the estimated conductivity and the actual conductivity, respectively.

Figure 14 represents the three histograms of the aluminum conductivity estimation error, corresponding to the solder conductivity factor  $\alpha_{solder} = 4, 6, 8$ , respectively. In the same way, Figure 15 represents the three histograms of the solder conductivity estimation error. It can be noted that the error of all estimated conductivities is below 4%. Particularly, the error of estimation of aluminum conductivity is higher than that of solder conductivity. This difference can be explained by the influence of the selected frequency band. Indeed, the maximal frequency of 2.5 MHz is not high enough to be solely sensitive to the aluminum layer. Therefore the EC data contain information of both the solder layer and the aluminum layer all over the used frequency band. Thus to improve the estimation results

in the aluminum layer, the maximal frequency should be increased so that at high frequencies, the influence of the solder layer would be negligible. In Figure 15, we note that the most aged configuration of the solder layer corresponding to the lowest conductivity provides the highest error of estimation. This may be due to the fact that because of the decrease of solder conductivity, the electromagnetic interaction between the EC probe and the solder layer becomes weaker, thus EC data is less sensitive to the solder layer of lower conductivity. In this case, to improve the results of estimation in the solder layer, the minimal frequency of investigation should be decreased.

Thus, the results of estimation show that by exploiting the simulated EC data featuring noise corresponding to a 60 dB SNR, we can estimate the evolution of ageing state of both aluminum and solder layers using an ANN. These preliminary results are very encouraging and invite us to apply this method to data provided by the experiment on actual power module samples.

#### 4. CONCLUSIONS AND PERSPECTIVES

The paper focuses on the estimation of conductivity variation in the multilayered structure of a power semiconductor module using the EC method during an ageing process. The authors have used the ANN to estimate the conductivity variations of the aluminum and the solder layers in the power module by exploiting the simulation data of electromagnetic coupling between the EC probe and the multilayered structure of power module. The data used on this study are simulated EC data provided by FE computations. They are computed for different ageing configurations corresponding to conductivity changes appearing in two metallic layers (aluminum and solder). The results indicate that the implemented ANN allows estimating the conductivity of aluminum layer and solder layer with an estimation error less than 4%. The study demonstrates that the EC method is relevant for the estimation of the ageing state of power modules.

Further research will focus on the experimental validation of the methods. Once the variation of aluminum and solder conductivity are validated on a real power semiconductor module, the development of integrated EC systems dedicated to the health monitoring of power electronic components will be envisaged.

#### REFERENCES

1. Lutz, J., T. Hermann, M. Feller, R. Bayerer, T. Licht, and R. Amro, "Power cycling induced failure mechanisms in the viewpoint of rough temperature environment," *Proceedings of the 5th International Conference on Integrated Power Electronic Systems*, 55–58, Nuremberg, Mar. 2008.
2. Ciappa, M., "Selected failure mechanisms of modern power modules," *Microelectronics Reliability*, Vol. 42, Nos. 4–5, 653–667, 2002.
3. Martineau, D., T. Mazeaud, M. Legros, P. Dupuy, C. Levade, and G. Vanderschaeve, "Characterization of ageing failures on power MOSFET devices by electron and ion microscopies," *Microelectronics Reliability*, Vol. 49, Nos. 9–11, 1330–1333, 2009.
4. Detzel, T., M. Glavanovics, and K. Weber, "Analysis of wire bond and metallisation degradation mechanisms in DMOS power transistors stressed under thermal overload conditions," *Microelectronics Reliability*, Vol. 44, Nos. 9–11, 1485–1490, 2004.
5. Smet, V., F. Forest, J. Huselestein, A. Rashed, and F. Richardeau, "Evaluation of  $V_{CE}$  monitoring as a real time method to estimate ageing of bon wire — IGBT modules Stressed by power cycling," *IEEE Transactions on Industrial Electronics*, Vol. 60, No. 7, 2760–2770, 2013.
6. Pietranico, S., S. Lefebvre, S. Pommier, and M. Berkani Bouaroudj, "A study of the effect of degradation of the aluminum metallization layer in the case of power semiconductor devices," *Microelectronics Reliability*, Vol. 51, Nos. 9–11, 1824–1829, 2011.
7. Udpa, S. and P. Moore, *Nondestructive Testing Handbook*, 3rd Edition, Vol. 5, Electromagnetic Testing, The American Society for Nondestructive Testing, 2004.
8. Ravat, C., P.-Y. Joubert, Y. Le bihan, C. Marchand, M. Woytasik, and E. Dufour-Gergam, "Non-destructive evaluation of small defects using an eddy current microcoil sensor array," *Sensor Letter*, Vol. 7, No. 3, 400–405, 2009.

9. Nguyen, T. A., P.-Y. Joubert, S. Lefebvre, G. Chaplier, and L. Rousseau, "Study for the non-contact characterization of metallization ageing of power electronic semiconductor device using the eddy current technique," *Microelectronics Reliability*, Vol. 51, No. 6, 1127–1135, 2011.
10. Nguyen, T. A., P.-Y. Joubert, S. Lefebvre, and S. Bontemps, "Monitoring of ageing chips of semiconductor power modules using eddy current sensor," *Electronics Letters*, Vol. 49, No. 6, 415–417, 2013.
11. Rojas, R., *Neural Networks: A Systematic Introduction*, Springer, Berlin, 1996.
12. Vernon, S.-N., "The universal impedance diagram of the ferrite pot core eddy current transducer," *IEEE Transactions on Magnetics*, Vol. 25, No. 3, 2639–2645, 1989.
13. Le Bihan, Y., "Study on the transformer equivalent circuit of eddy current nondestructive evaluation," *NDT&E International*, Vol. 36, No. 5, 297–302, 2003.
14. Bore, T., P.-Y. Joubert, and D. Placko, "A differential DPSM based modeling applied to eddy current imaging problems," *Progress In Electromagnetics Research*, Vol. 148, 209–221, 2014.
15. Cacciola, M., F. C. Morabito, D. Polimeni, and M. Versaci, "Fuzzy characterization of flawed metallic plates with eddy current tests," *Progress In Electromagnetics Research*, Vol. 72, 241–252, 2007.
16. Joubert, P.-Y., E. Vourc'h, and V. Thomas, "Experimental validation of an eddy current probe dedicated to the multi-frequency imaging of bore holes," *Sensors and Actuators A*, Vol. 185, 132–138, 2012.
17. Hasanzadeh, R. P. R., A. R. Moghaddamjoo, S. H. H. Sade Ghi, A. H. Rezaie, and M. Ahmadi, "Optimal signal-adaptive maximum likelihood filter for enhancement of defects in eddy current C-scan images," *NDT&E International*, Vol. 41, No. 5, 371–377, 2008.
18. Yusa, N., N. Huang, and K. Miya, "Numerical evaluation of the ill-posedness of eddy current problems to size real cracks," *NDT&E International*, Vol. 40, No. 3, 185–191, 2007.
19. Agatonovic, M., Z. Stankovic, I. Milovanovic, N. Doncov, L. Sit, T. Zwick, and B. Milovanovic, "Efficient neural network approach for 2D DOA estimation based on antenna array measurements," *Progress In Electromagnetics Research*, Vol. 137, 741–758, 2013.
20. Wefky, A., F. Espinosa, L. D. Santiago, A. Gardel, P. Revenga, and M. Martinez, "Modeling radiated electromagnetic emissions of electric motorcycles in terms of driving profile using MLP neural networks," *Progress In Electromagnetics Research*, Vol. 135, 231–244, 2013.
21. Hornik, K., M. Stinchcombe, and H. White, "Multilayer feed-forward networks are universal approximators," *Neural Networks*, Vol. 2, No. 5, 359–366, 1989.
22. Peng, X., "Eddy current crack extension direction evaluation based on neural network," *Proceedings of IEEE Sensors*, 1–4, 2012.
23. Vourc'h, E., P.-Y. Joubert, G. Le Gac, and P. Larzabal, "Nondestructive evaluation of loose assemblies using multi-frequency eddy currents and artificial neural networks," *Measurement Science and Technology*, Vol. 24, No. 12, 7 Pages, 2013.
24. Demuth, H. and M. Beale, *Neural Network Toolbox for Use with MATLAB*, User's Guide, Version 4, Sep. 2000.
25. Levenberg, K., "A method for the solution of certain non-linear problems in least squares," *Quarterly Journal of Applied Mathematics*, Vol. II, No. 2, 164–168, 1944.
26. Hagan, M. T. and M. Menhaj, "Training feed-forward networks with the Levenberg-Marquardt algorithm," *IEEE Transactions on Neural Networks*, Vol. 5, No. 6, 989–993, 1994.
27. Smith, M., *Neural Network for Statistical Modeling*, Van Nostrand-Reinhold, New York, 1993.